## PAPER

CrossMark
click for updates

# Facile synthesis of ultrathin MoS$_2$/C nanosheets for use in sodium-ion batteries

Minchan Li,†[a] Zhe Wu,†[b] Zhenyu Wang,[a] Sicen Yu,[a] Yinggang Zhu,[a] Bo Nan,[a] Yang Shi,[a] Yingying Gu,[b] Hongtao Liu,[b] Yougen Tang[b] and Zhouguang Lu*[a]

We present a clean and simple method for the synthesis of MoS$_2$/C hybrids. Commercial ion-exchange resins are used to absorb aqueous molybdate, followed by annealing with sulfur powder in an inert atmosphere. Even ultrathin MoS$_2$ nanosheets with enlarged interlayers (0.63 nm) are homogeneously wrapped by mesoporous graphitic carbon. When evaluated as anodes for sodium-ion batteries, the MoS$_2$/C nanocomposite exhibits good electrochemical performance. The first discharge/charge capacities at current density 50 mA g$^{-1}$ are 784.3 and 590.0 mA h g$^{-1}$, respectively, with initial coulombic efficiency of approximately 75%. It exhibits superior rate capabilities, with specific discharge capacities of 513.1, 467.3, 437.1, 399.2, 361.8, and 302.7 mA h g$^{-1}$ at current densities of 50, 100, 200, 500, 1000, and 2000 mA g$^{-1}$, respectively. This superior electrochemical performance is mainly due to the synergistic effect between the uniformly-distributed, ultrathin MoS$_2$ nanosheets and the highly graphitized carbon. This not only mitigates mechanical stress during repeated cycling, but also provides good conductivity.

## Introduction

Energy storage has become a growing global concern over the past few decades because of increasing energy demand. The most common rechargeable batteries, used in almost all portable electronic devices, are of the lithium-ion type. Although the technology is quite mature, there are remaining concerns regarding battery safety, lifetime, poor low-temperature performance and cost. As the use of large format lithium batteries becomes widespread, the demand for Li metal will greatly increase. This, in addition to the restricted distribution of Li mineral reserves, may dramatically increase the cost of lithium ion batteries.[1,2] Rechargeable sodium ion batteries (SIBs) have recently attracted great attention due to the wide availability of sodium. Since sodium is abundant and possesses similar physical and chemical properties to lithium, sodium-based batteries could provide a cheaper alternative compared to lithium ones.[3,4] It has the possibility to provide low cost, large format batteries with the potential to meet the requirements of large scale, grid-connected energy storage facilities. A large number of anode materials, such as transitional metal oxides,[5,6] carbon-based materials[7] and Na-alloys[8] have been studied for use in sodium-ion batteries.

[a]*Department of Materials Science and Engineering, South University of Science and Technology of China, Shenzhen, Guangdong 518055, China. E-mail: luzg@sustc.edu.cn*

[b]*School of Chemistry and Chemical Engineering, Central South University, Changsha, Hunan 410083, China*

† These authors contributed equally.

Unfortunately, the intrinsic large ionic radius and heavy molar mass of Na$^+$ has restricted the specific capacity, cycling stability and rate capability of SIBs.[9,10]

Recently, there is growing research interest in transition metal dichalcogenides (TMDs) for their special layered structure which maintains its structural integrity, stability and volume, even after being housed in sodium-ion batteries.[11] Among them, MoS$_2$ is attractive due to its favorable Na-intercalation structure at certain potentials, and high reversible capacity (670 mA h g$^{-1}$).[12] In particular, it has a well-defined layered structure, where the 2D plane consists of three atomic layers of S–Mo–S. It has also been reported that interlayer-expanded MoS$_2$ can improve Na$^+$ diffusion kinetics and benefit sodiation/desodiation processes.[13] However, the practical application of MoS$_2$ is still limited, as existing MoS$_2$ layers tend to restack due to van der Waals interactions, leading to decreases in active sites accessible to Na$^+$. Additionally, the low electronic conductivity of MoS$_2$ does not favor electrode reactions. Furthermore, volume variation in MoS$_2$ particles causes them to break apart and have poor inter-particle contact.[14,15] To overcome these problems, many efforts have been devoted to improving the electrochemical performance of MoS$_2$ by combining it with conductive materials. Choi et al.[16] recently created 3D MoS$_2$–graphene microspheres by employing polystyrene beads as templates, which showed high capacity retention and enhanced cycling stability. Xiong's group synthesized flexible MoS$_2$/C nanofibers by electrospinning. When evaluated as a binder-free electrode, the material demonstrated high reversible capacity (381.7 mA h g$^{-1}$ at 0.1 A g$^{-1}$) and superior

rate capability.[17] Maier's group improved the conversion-type reaction by employing ultrasmall $MoS_2$ nanoplates in carbon nanofibers.[18] The as prepared sample displayed a remarkable discharge capacity of 436 mA h g$^{-1}$ at 1 A g$^{-1}$. However, the capacity dropped to 57% after 100 cycles. Bang *et al.* optimized the cycling performance with nearly no capacity loss for 100 cycles by using layered $MoS_2$ nanosheets and controlling the terminal voltage to 0.4 V.[19] The discharge capacity of their device was only 165 mA h g$^{-1}$, thus improving the discharge capacity is still an urgent task. Wang *et al.* successfully prepared flower-like $MoS_2$/C nanospheres deliver a high reversible capacity of 520 mA h g$^{-1}$ at a current density of 0.1C. After increasing the current density to 1C, $MoS_2$/C nanospheres still maintain a specific capacity of 400 mA h g$^{-1}$ for 300 cycles.[20] However, the expensive and complex processing steps will limit the applicability of this approach.

In this article, we report a simple and effective strategy for the *in situ* synthesis of $MoS_2$ nanosheets in porous graphitic carbon for use as anodes for sodium-ion batteries. Firstly, we prepared transition metal carbides/graphitic carbon hybrids (MoC/C nanocomposite) by utilizing ion exchange resins that absorb aqueous molybdate, followed by annealing treatment in an inert atmosphere. Simultaneously, carbon that was thermally decomposed from resin was converted to highly-ordered and porous graphitic carbon *via* the catalytic action of Mo species, which greatly improved the conductivity of nanocomposite. Then, we obtained $MoS_2$/graphitic carbon hybrids ($MoS_2$/C nanocomposite) by annealing a mixture of MoC/C nanocomposite and sulfur powder. The structure of $MoS_2$/C nanocomposite exhibits outstanding electrochemical performance. We attribute their high reversible discharge capacity and relatively stable cycling properties to their unique structure – where ultrathin $MoS_2$ nanosheets are supported on porous graphitic carbon. The structure allows enough space to relieve volume expansion and mechanical stresses brought about by sodium-ion absorption, thereby guaranteeing stability and reversibility. Meanwhile, the high conductivity of the carbon-based material ensures outstanding rate capability at various current densities.

## Experimental section

### Preparation of MoC/C and $MoS_2$/C nanocomposite

Polymethacrylate-based anion-exchange resins (D 314) were first rinsed with absolute ethanol for 10 hours to remove adsorbed organic components. The resins were then washed successively with 5% HCl, deionized water, and 5% NaOH solution three times. Subsequently, the wet resins were dried in a vacuum oven at 60 °C for 12 h. After soaking and stirring in 0.1 mol L$^{-1}$ $(NH_4)_6Mo_7O_{24}$ solution for 6 h, the resins were cleaned with deionized water three times continuously to wash away redundant ions from their surfaces.[21,22]

Thereafter, the dried Mo-containing resins were transferred into a ceramic boat and annealed at a temperature of 700 °C for 2 h under a flow of inert atmosphere (150 mL min$^{-1}$). After cooling to ambient temperature, the products were ground and sieved through a 80–140 mesh. Finally, $MoS_2$/C nanocomposite
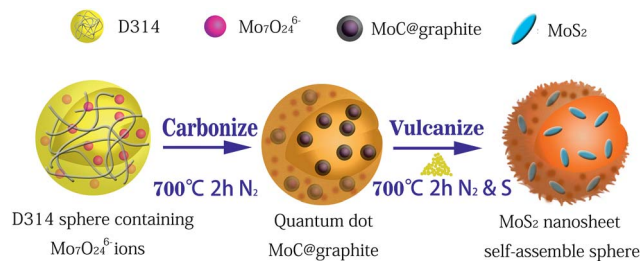


Fig. 1 Schematic representation showing synthesis of $MoS_2$/C nanocomposite.

was obtained by mixing the as-prepared MoC/C and sulfur powders, followed by the same calcining process mentioned above. The whole preparation procedure is schematically illustrated in Fig. 1.

### Characterization

The crystallinity of samples was analyzed by a Siemens X-ray generator with Cu Kα radiation ($\lambda = 0.15406$ nm) in the range of 10–80°. Raman spectroscopy measurement was performed in a LabRAM HR 800 Raman microscope using an excitation laser beam with a wavelength of 532 nm. The specific surface areas of the sample were analyzed by nitrogen ($N_2$) adsorption–desorption isotherms at 77 K using a NOVA 1200e Surface Area. Morphology characterization and energy dispersive spectrometry analysis of samples were carried out with a field-emission scanning electron microscope (SEM; Hitachi, S4800). Further characterization was obtained from a field-emission transmission electron microscope (TEM; JEOL Ltd, Tokyo, Japan) at 200 kV.

### Electrochemical measurements

The working electrode was prepared by mixing active material (80 wt%), acetylene black (10 wt%) and polyvinylidene difluoride (PVDF) (10 wt%) in *N*-methyl-2-pyrrolidone (NMP) solution to form a homogeneous slurry, which was then pasted uniformly onto copper foil and dried for 12 h at 120 °C. The half-cell was assembled in an Ar-filled glove box (Mbraun, $H_2O$ and $O_2 < 0.1$ ppm) by taking the circular copper plate as a cathode, glass fiber as a separator and pure Na foil as an anode. The sodium foils were used as counter electrodes and reference electrodes. Glass fiber was applied as a separator. The electrolyte was composed of a solution of 1 M $NaClO_4$ in ethylene carbonate (EC)–propylene carbonate (PC)–fluoroethylene carbonate (FEC) (EC : PC = 1 : 1 volume ratio, FEC = 5 wt%). The electrochemical performances of the half cells were characterized by cyclic voltammetry and galvanostatic charge–discharge.

## Results and discussion

Fig. 2 shows the X-ray diffraction (XRD) patterns of MoC/C and $MoS_2$/C. The crystallographic structure of the MoC/C nanocomposite is displayed in Fig. 2b. All the diffraction peaks
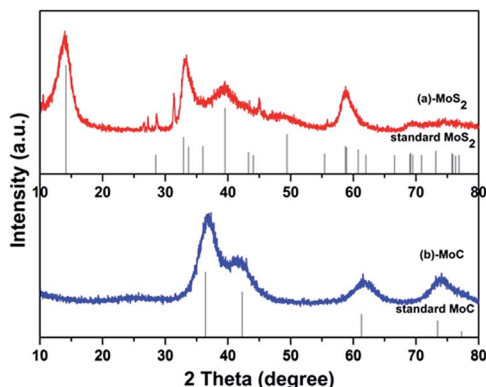
**Fig. 2** XRD patterns of prepared (a) MoC/C nanocomposite and MoC standard, and (b) $MoS_2$/C nanocomposite and $MoS_2$ standard.

match well with those of a MoC standard (JCPD no. 65-0280), indicating high sample purity. The $MoS_2$/C nanocomposite shows conspicuous, sharp peaks at 14.2°, 32.9° and 39.5° (Fig. 2a), which are indexed as (002), (100) and (103) facets of $MoS_2$ (JCPD no. 75-1539), indicating that the prepared samples have high crystallinity. Any small impurity peaks are negligible.

Raman spectra provide an easy, qualitative characterization of $MoS_2$ nanosheets (Fig. 3a). The typical peak, known as the $E_{2g}^1$, originates from the in-plane vibration of Mo–S, and an $A_{1g}$ peak from out-of-plane vibrations is also observed.[20,23] Meanwhile, two distinguishable peaks are observed at 1345 and 1590 cm$^{-1}$, which can be ascribed to the D-band and G-band of carbon, respectively. The peak intensity ratio ($I_D/I_G$) is a useful index for the degree of crystallinity of carbon materials. The smaller the ratio, the higher the degree of ordering.[24] As shown in Fig. 3b, the specific surface area of the as-prepared $MoS_2$ nanosheets is calculated by the conventional Brunauer–Emmett–Teller (BET) method, and is approximately 59.34 m$^2$ g$^{-1}$. We also performed the XPS measurements. In Fig. 3c, the Mo 3d peaks are assigned to Mo$^{4+}$ 3d$_{5/2}$ (229.3 eV) and Mo$^{4+}$ 3d$_{3/2}$ (232.6 eV), which are expected values for Mo$^{4+}$ in the $MoS_2$.

The corresponding S 2p peak consists of a single doublet of 2p$_{1/2}$ (163.4 eV) and S 2p$_{3/2}$ (162.3 eV), consistent with the S$^{2-}$ type present in $MoS_2$ (Fig. 3d). It shows a small peak at around 236 eV, which corresponds to Mo$^{6+}$ 3d$_{5/2}$ from Mo oxidation.[25]

The SEM and TEM images of $MoS_2$/C are shown in Fig. 4. The SEM images (Fig. 4a), show the samples to be clustered together with a flower-like morphology. Each cluster is approximately 200 nm in diameter. The energy dispersive spectrum further confirms the existence of Mo, S, and C. Fig. 4c and d show the TEM and HRTEM images of $MoS_2$/C. It is clear that each cluster consists of a large number of $MoS_2$ nanosheets, which are located in the carbon matrix. These ultrathin nanosheets have lengths of 20 nm and widths of 10 nm. Distinct diffraction rings are visible in the inset of Fig. 4c, and the clear lattice fringes with 0.63 nm spacing (Fig. 4d) indicate that the $MoS_2$ is well crystallized. The graphitic carbon layer of the composites is about 3 nm, and it is clearly to see the lattice fringes of graphite.

Fig. 5a displays a typical CV curve of the $MoS_2$/C nanocomposite in the potential window of 0.01–3.0 V. Three reduction peaks in the first sodiation process are observed, situated at 1.77, 0.82, and 0.12 V, respectively. The reduction peak at 1.7 V is attributed to the insertion of Na$^+$ into $MoS_2$, forming Na$_x$MoS$_2$.[26,27] The next reduction peak, at 0.82 V, is related to the further insertion of Na$^+$ in combination with the formation of an interphase layer of solid electrolyte. The sharp peak at 0.15 V indicates a conversion reduction (Na$_x$MoS$_2$ + Na$^+$ → Mo + Na$_x$S).[20,28] In the following oxidation curve, the peak near 1.85 V corresponds to desodiation. Interestingly, the 2nd, 3rd and 4th CV curves nearly overlap, indicating good reversibility and predominance of storage reduction. We can attribute the high reversibility and stability of sodiation/disodiation to the layered structure of $MoS_2$ nanosheets, and to the porous graphitic carbon which possesses sufficient space to provide structural stability, effectively preventing the structure from collapsing and disintegrating.

The galvanostatic discharge/charge behavior of the $MoS_2$/C nanocomposite was measured at currents of 50 mA g$^{-1}$ and 500 mA g$^{-1}$, respectively. As shown in Fig. 5b, the first discharge process contains correlative plateau regions that are identified
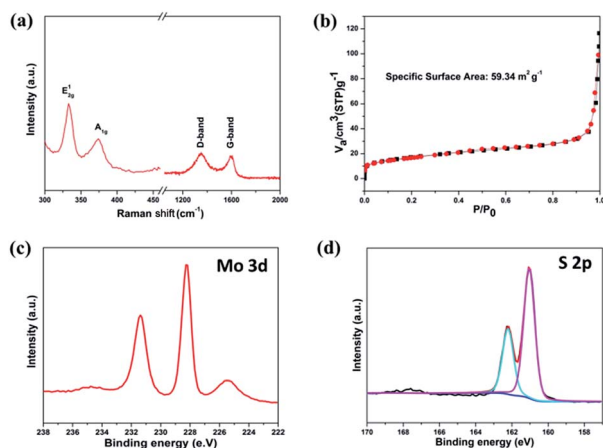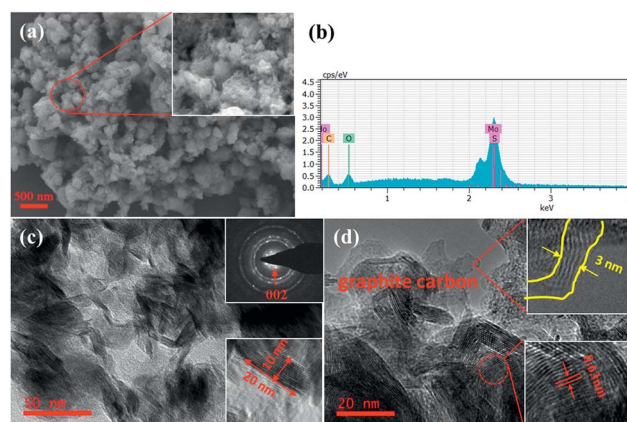


**Fig. 3** (a) Raman spectra of $MoS_2$/C, (b) N$_2$ adsorption/desorption isotherms of $MoS_2$/C, (c) Mo 3d and (d) S 2p XPS spectra of the $MoS_2$ nanosheets.



**Fig. 4** $MoS_2$/C nanocomposite characterized by (a) SEM image, (b) energy dispersive spectrum, (c) TEM images, and (d) HRTEM image.
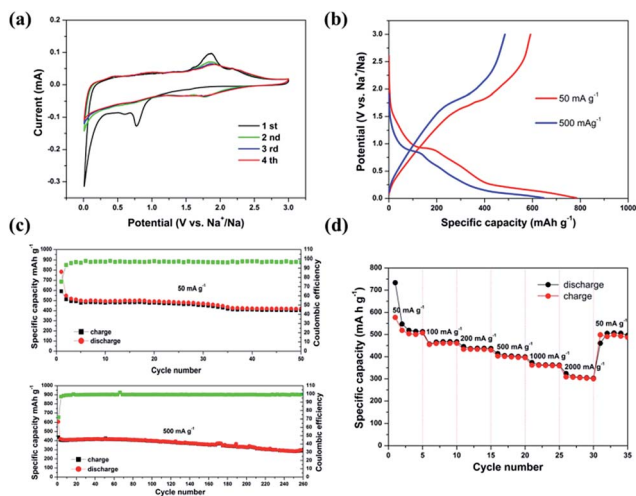
**Fig. 5** Electrochemical performance of the MoS$_2$/C nanocomposite: (a) CV curves at scan rate 0.1 mV s$^{-1}$; (b) first galvanostatic discharge/charge profiles at current densities 50 and 500 mA g$^{-1}$; (c) cycling performance and corresponding coulombic efficiency; and (d) rate capacity at different current densities.

to the CV profiles. The initial discharge/charge capacities of the MoS$_2$/C nanocomposite at 50 mA g$^{-1}$ are 784.3 and 590.0 mA h g$^{-1}$, respectively, with a coulombic efficiency of 75.5%. At the current density of 500 mA g$^{-1}$, the initial discharge/charge capacities are 646.4 and 484.8 mA h g$^{-1}$, corresponding to a coulombic efficiency of 75%. Fig. 5c further exhibits the cycling performance of the MoS$_2$/C nanocomposite. Apparently, the as-prepared sample demonstrates good cycle retention at both current densities of 50 mA g$^{-1}$ and 500 mA g$^{-1}$. The discharge capacity is maintained at 418.8 mA h g$^{-1}$ at 50 mA g$^{-1}$ after 50 cycles. Even at bigger current density of 500 mA g$^{-1}$, it can still remain the capacity of 295.0 mA h g$^{-1}$ after 260 cycles. As expected, the MoS$_2$/C nanocomposite also exhibits excellent rate capacity (Fig. 5d). When the current density is increased from 50 mA g$^{-1}$ to 2000 mA g$^{-1}$, it simultaneously displays promising specific capacities and rate capabilities. The reversible capacities at 50, 100, 200, 500, 1000, 2000 mA g$^{-1}$ are 513.1, 467.3, 437.1, 399.2, 361.8, 302.7 mA h g$^{-1}$, respectively. Importantly, when the current density resumes to 50 mA g$^{-1}$ after cycling at different rates, a capacity of 505.7 mA h g$^{-1}$ is still achieved. This further confirms the stable structure of the nanosheet-based hybrid and its excellent reversibility.

## Conclusions

In this study, a novel and simple method is proposed for preparation of layered MoS$_2$/C nanosheets by calcining sulfur powders and MoC/C hybrids in an inert atmosphere. The MoC/C hybrids were synthesized from an ion-exchange, resin-adsorbing solution containing heavy metal salts. Based on the above characterization, results and electrochemical investigations, the MoS$_2$/C composite displayed satisfactory electrochemical performance and structural integrity. The MoS$_2$/C nanocomposite was composed of ultrathin nanosheets

($\approx 10$ nm) uniformly distributed on a porous conductive carbon matrix. This structure not only provides sufficient ionic and electronic transport, but also mitigates mechanical stress on MoS$_2$ during discharge and charge. Meanwhile, the confined, ultrathin, layered MoS$_2$ nanosheets can effectively inhibit aggregation and facilitate electrode reactions. The synergetic effect of MoS$_2$ nanosheets with a porous carbon matrix results in outstanding properties – even after 50 cycles, the capacity remains at 418.8 mA h g$^{-1}$ with a current density of 50 mA g$^{-1}$, and at 300.4 mA h g$^{-1}$ with a current density of 500 mA g$^{-1}$. This strategy presented in this paper may also improve the electrochemical performance of other metal sulfides with potential for use as sodium-ion battery anodes.

## Notes and references

1 P. Poizot, S. Laruelle, S. Grugeon, L. Dupont and J. Tarascon, *Nature*, 2000, **407**, 496–499.
2 M. D. Slater, D. Kim, E. Lee and C. S. Johnson, *Adv. Funct. Mater.*, 2013, **23**, 947–958.
3 V. Palomares, P. Serras, I. Villaluenga, K. B. Hueso, J. Carretero-González and T. Rojo, *Energy Environ. Sci.*, 2012, **5**, 5884–5901.
4 H. Pan, Y. S. Hu and L. Chen, *Energy Environ. Sci.*, 2013, **6**, 2338–2360.
5 Q. Sun, Q. Q. Ren, H. Li and Z. W. Fu, *Electrochem. Commun.*, 2011, **13**, 1462–1464.
6 L. Zhao, H. L. Pan, Y. S. Hu, H. Li and L. Q. Chen, *Chin. Phys. B*, 2012, **21**, 028201.
7 D. Stevens and J. Dahn, *J. Electrochem. Soc.*, 2000, **147**, 4428–4431.
8 S. Komaba, Y. Matsuura, T. Ishikawa, N. Yabuuchi, W. Murata and S. Kuze, *Electrochem. Commun.*, 2012, **21**, 65–68.
9 R. Tenne, *Adv. Mater.*, 1995, **7**, 965–995.
10 (*a*) Y. Li, Z. Zhou, S. Zhang and Z. Chen, *J. Am. Chem. Soc.*, 2008, **130**, 16739–16744; (*b*) H. Ramakrishna Matte, A. Gomathi, A. K. Manna, D. J. Late, R. Datta, S. K. Pati and C. Rao, *Angew. Chem.*, 2010, **122**, 4153–4156.
11 (*a*) J. S. Kim, H. J. Ahn, H. S. Ryu, D. J. Kim, G. B. Cho, K. W. Kim, T. H. Nam and J. H. Ahn, *J. Power Sources*, 2008, **178**, 852–856; (*b*) A. Kitajou, J. Yamaguchi, S. Hara and S. Okada, *J. Power Sources*, 2014, **247**, 391–395; (*c*) D. Su, S. Dou and G. Wang, *Chem. Commun.*, 2014, **50**,

4192–4195; (d) B. Qu, C. Ma, G. Ji, C. Xu, J. Xu, Y. S. Meng, T. Wang and J. Y. Lee, *Adv. Mater.*, 2014, **26**, 3854–3859.

12 X. Huang, Z. Zeng and H. Zhang, *Chem. Soc. Rev.*, 2013, **42**, 1934–1946.

13 Y. P. Lei, Q. Shi, C. Han, B. Wang, N. Wu, H. Wang and Y. D. Wang, *Nano Res.*, 2016, **9**, 2498–2509.

14 X. Xie, Z. Ao, D. Su, J. Zhang and G. Wang, *Adv. Funct. Mater.*, 2015, **25**, 1393–1403.

15 P. P. Wang, H. Sun, Y. Ji, W. Li and X. Wang, *Adv. Mater.*, 2014, **26**, 964–969.

16 S. H. Choi, Y. N. Ko, J. K. Lee and Y. C. Kang, *Adv. Funct. Mater.*, 2015, **25**, 1780–1788.

17 J. X. Liu, H. Cao, B. Jiang, Y. H. Xue, L. Fu, D. Hou and Y. Huang, *Sci. China Mater.*, 2016, **59**, 459–474.

18 C. Zhu, X. Mu, P. A. van Aken, Y. Yu and J. Maieret, *Angew. Chem., Int. Ed.*, 2014, **53**, 2152–2156.

19 G. S. Bang, K. W. Nam, J. Y. Kim, J. Shin, J. W. Choi and S. Y. Choi, *ACS Appl. Mater. Interfaces*, 2014, **6**, 7084–7089.

20 J. Wang, C. Luo, T. Gao, A. Langrock, A. C. Mignerey and C. S. Wang, *Small*, 2015, **11**, 473–481.

21 P. Tao, J. Hu, W. Wang, S. Wang, M. Li, H. Zhong, Y. Tang and Z. Lu, *RSC Adv.*, 2014, **4**, 13518–13524.

22 J. Hu, P. Tao, S. Wang, Y. Liu, Y. Tang, H. Zhong and Z. Lu, *J. Mater. Chem. A*, 2013, **1**, 6558–6562.

23 H. S. Lee, S. W. Min, Y. G. Chang, M. K. Park, T. Nam, H. Kim, J. H. Kim, S. Ryu and S. Im, *Nano Lett.*, 2012, **12**, 3695–3700.

24 S. Urbonaite, L. Hälldahl and G. Svensson, *Carbon*, 2008, **46**, 1942–1947.

25 G. S. Bang, K. W. Nam and J. Y. Kim, *ACS Appl. Mater. Interfaces*, 2014, **6**, 7084–7089.

26 L. David, R. Bhandavat and G. Singh, *ACS Nano*, 2014, **8**, 1759–1770.

27 Z. Hu, Q. N. Liu, W. Y. Sun, W. J. Li, Z. L. Tao, S. L. Chou, J. Chen and S. X. Dou, *Inorg. Chem. Front.*, 2016, **3**, 532–535.

28 Z. Hu, L. Wang, K. Zhang, J. Wang, F. Cheng, Z. Tao and J. Chen, *Angew. Chem.*, 2014, **126**, 13008–13012.